A Section 508–conformant HTML version of this article is available at https://doi.org/10.1289/EHP14132.

Multiomics Analysis of PCB126's Effect on a Mouse Chronic-Binge Alcohol Feeding Model

Tyler C. Gripshover,[1,2,3] Banrida Wahlang,[1,2,3,4] Kimberly Z. Head,[2,5] Jianzhu Luo,[2] Oluwanifemi E. Bolatimi,[1] Melissa L. Smith,[4,6] Eric C. Rouchka,[6,7] Julia H. Chariker,[7,8] Jason Xu,[9] Lu Cai,[1,4,9] Timothy D. Cummins,[10] Michael L. Merchant,[1,4,10,12] Hao Zheng,[4] Maiying Kong,[4,11,12,13] and Matthew C. Cave[1,2,3,4,5,6,12,14,15]

[1]Department of Pharmacology and Toxicology, University of Louisville School of Medicine, Louisville, Kentucky, USA
[2]Division of Gastroenterology, Hepatology and Nutrition, Department of Medicine, School of Medicine, University of Louisville, Louisville, Kentucky, USA
[3]University of Louisville Superfund Research Program, University of Louisville, Louisville, Kentucky, USA
[4]The Center for Integrative Environmental Health Sciences, University of Louisville, Louisville, Kentucky, USA
[5]Hepatobiology & Toxicology COBRE, University of Louisville School of Medicine, Louisville, Kentucky, USA
[6]Department of Biochemistry and Molecular Genetics, University of Louisville School of Medicine, Louisville, Kentucky, USA
[7]Kentucky IDeA Network of Biomedical Research Excellence (KY INBRE) Bioinformatics Core, University of Louisville, Louisville, Kentucky, USA
[8]Department of Neuroscience Training, University of Louisville, Louisville, Kentucky, USA
[9]Department of Pediatrics, Pediatric Research Institute, University of Louisville School of Medicine, Louisville, Kentucky, USA
[10]Division of Nephrology and Hypertension, Department of Medicine and Clinical Proteomics Center, University of Louisville, Louisville, Kentucky, USA
[11]Department of Bioinformatics and Biostatistics School of Public Health and Information Sciences, University of Louisville, Louisville, Kentucky, USA
[12]University of Louisville Alcohol Research Center, University of Louisville, Louisville, Kentucky, USA
[13]Brown Cancer Center, University of Louisville, Louisville, Kentucky, USA
[14]The Robley Rex Veterans Affairs Medical Center, Louisville, Kentucky, USA
[15]The Liver Transplant Program at UofL Health – Jewish Hospital Trager Transplant Center, Louisville, Kentucky, USA

Background: Environmental pollutants, including polychlorinated biphenyls (PCBs) have been implicated in the pathogenesis of liver disease. Our group recently demonstrated that PCB126 promoted steatosis, hepatomegaly, and modulated intermediary metabolism in a rodent model of alcohol-associated liver disease (ALD).

Objective: To better understand how PCB126 promoted ALD in our previous model, the current study adopts multiple omics approaches to elucidate potential mechanistic hypotheses.

Methods: Briefly, male C57BL/6J mice were exposed to 0.2 mg/kg polychlorinated biphenyl (PCB) 126 or corn oil vehicle prior to ethanol (EtOH) or control diet feeding in the chronic-binge alcohol feeding model. Liver tissues were collected and prepared for mRNA sequencing, phosphoproteomics, and inductively coupled plasma mass spectrometry for metals quantification.

Results: Principal component analysis showed that PCB126 uniquely modified the transcriptome in EtOH-fed mice. EtOH feeding alone resulted in >4,000 differentially expressed genes (DEGs), and PCB126 exposure resulted in more DEGs in the EtOH-fed group (907 DEGs) in comparison with the pair-fed group (503 DEGs). Top 20 significant gene ontology (GO) biological processes included "peptidyl tyrosine modifications," whereas top 25 significantly decreasing GO molecular functions included "metal/ion/zinc binding." Quantitative, label-free phosphoproteomics and western blot analysis revealed no major significant PCB126 effects on total phosphorylated tyrosine residues in EtOH-fed mice. Quantified hepatic essential metal levels were primarily significantly lower in EtOH-fed mice. PCB126-exposed mice had significantly lower magnesium, cobalt, and zinc levels in EtOH-fed mice.

Discussion: Previous work has demonstrated that PCB126 is a modifying factor in metabolic dysfunction-associated steatotic liver disease (MASLD), and our current work suggests that pollutants also modify ALD. PCB126 may, in part, be contributing to the malnutrition aspect of ALD, where metal deficiency is known to contribute and worsen prognosis. https://doi.org/10.1289/EHP14132

Introduction

Alcohol-associated liver disease (ALD) is a major cause of preventable disease[1,2] and a leading reason for liver transplantation[3] in the United States. ALD and its comorbidities are increasing economic costs, hospitalizations,[4] and mortality and are projected to continue to rise for the next two decades.[5] During the SARS-CoV-2 pandemic, it was reported that a substantial increase of alcohol use and alcohol-related emergencies occurred during and shortly after the lockdown quarantine.[6,7] Excessive alcohol consumption is the primary etiology for ALD development, where drinking patterns and standard drinks (grams of EtOH per drink) have been described.[8] This disease manifests along the steatotic liver disease (SLD) spectrum beginning with simple hepatic steatosis that can progress with accompanied inflammation and fibrotic scarring. Furthermore, ALD may advance to the point of end-stage liver disease, where decompensated cirrhosis and hepatocellular carcinoma may become part of a patient's prognosis.[9] Risk factors for ALD susceptibility and progression certainly exist and have previously been described.[10] For example, males, tobacco smoke,[10] *PNPLA3* polymorphisms,[11] and obesity[10,11] are risk factors that predispose individuals to ALD development and worsened disease. Another ALD risk factor of note is the aspect of malnutrition or undernutrition. Particularly, depletion of essential metals may occur during excessive alcohol consumption and contribute to ALD pathogenesis.[12,13] However, not all individuals with unhealthy drinking behaviors develop ALD.

The related liver disease, metabolic dysfunction-associated steatotic liver disease (MASLD, formerly nonalcoholic fatty liver disease) has been demonstrated to be altered or enhanced due to environmental pollutant exposures.[14–16] These observations are largely explained by the "two-hit" hypothesis where a second

Address correspondence to Matthew C. Cave, 505 S. Hancock St. 542D CTR Building, Louisville, KY 40202 USA. Telephone: (502) 852-5252; Fax: (502) 852-8927. Email: matt.cave@louisville.edu

Supplemental Material is available online (https://doi.org/10.1289/EHP14132).

The authors of this manuscript do not declare any conflicts of interest.

Conclusions and opinions are those of the individual authors and do not necessarily reflect the policies or views of EHP Publishing or the National Institute of Environmental Health Sciences.

Received 9 October 2023; Revised 13 March 2024; Accepted 14 March 2024; Published 15 April 2024.

insult is required to develop more severe MASLD.[17] Most commonly, environmental pollutants like polychlorinated biphenyls (PCBs) act as metabolism disrupters impacting liver intermediary metabolism. Importantly, toxicants have also been demonstrated to decrease essential metal micronutrient levels, including zinc (Zn),[18–20] selenium (Se),[18–20] and copper (Cu),[20] specifically in the liver. In addition, alcohol[21] and at least nondioxin-like polychlorinated biphenyls (PCBs)[22] have been associated with abnormal phosphoproteome changes. However, research studying ALD's subjection to enhanced disease severity by pollutant exposures are underappreciated and warrant additional studies. Like MASLD, ALD is subject to disease modifiers, including sex, race, diet, and patterns of alcohol consumption, that may promote pathogenesis.[23] Previous epidemiology studies have shown that pollutant exposure with concomitant high alcohol consumption rates is associated with higher odds ratio of hepatocellular cancer[24] and other disease risk.[25] More data are required on the disease-modifying effects of environmental exposures in ALD. We recently characterized a model in which mice were exposed to 0.2 mg/kg polychlorinated biphenyl (PCB) 126 prior to *ad libitum* alcohol feeding via a modified chronic-binge (10-plus-one) model.[26] In this work, PCB126 coexposure worsened EtOH-induced hepatic steatosis and altered hepatic carbohydrate, protein, and lipid metabolism. Albumin, a key biomarker of liver function was $\sim 50\%$ lower in coexposed mice. Although PCB126 activated the aryl hydrocarbon receptor (AhR) to impact xenobiotic and energy metabolism, other second-hit mechanisms are unknown.

The current study used mRNA sequencing (RNA-Seq) techniques to assist in the unbiased generation of mechanistic hypotheses related to PCB126's ability to enhance murine ALD. This investigation then led us to evaluate the phosphoproteome and the metallome to foster more specific mechanistic hypotheses to pursue in future studies. The objective of this study was to elucidate altered genes and enriched gene ontology (GO) biological and molecular function processes to generate more mechanistic hypotheses related to PCB126's ability to promote ALD. We hypothesized that unique differentially expressed genes (DEGs) and enriched GO processes will be identified, which will provide insight into how PCB126 may be promoting ALD.

Methods

Animal Study

The University of Louisville Institutional Animal Care and Use Committee (IACUC) approved animal use protocols and procedures (IACUC 21871). Ten-week-old, male, C57BL/6J mice were purchased from Jackson Laboratory (strain#: 000664). After receiving the study animals, five mice per cage were housed in a pathogen-free, temperature-controlled (23.9°C) room with a 12-h light–dark cycle, accredited by the Association for Assessment and Accreditation of Laboratory Animal Care (AAALAC). Mice were given 1 wk to acclimate to facility transfer and provided autoclaved rodent chow (5010; LabDiet) and *ad libitum* access to food and water. The current study is an exact repeat in terms of design for scientific rigor and tissue availability for omics analysis, which was described in our recent published work.[26] No changes were made in this repeat study when compared with the initial study. In brief, mice were orally gavaged once with either 0.2 mg/kg 3,3′,4,4′,5-Pentachlorobiphenyl (PCB126) (catalog: C-126N-5MG; AccuStandard) or corn oil vehicle (catalog: C8267-500ML; Millipore Sigma) prior to EtOH feeding. Stock 1 mg/mL PCB126 is stored at room temperature in a desiccator chamber. Stock PCB126 was diluted with corn oil vehicle on a rocker for 24 h to achieve working exposure dose of 0.02 mg/mL. Mice were orally gavaged based on body weight to achieve an exposure dose of 0.2 mg/kg. Study animals were then placed on the commonly used chronic-binge (10-plus-one) alcohol feeding model.[27] EtOH (95%) was purchased internally from the University of Louisville's stock room (catalog: 2816; Decon Labs Inc.). Mice provided the EtOH diet were given 5 d of acclimation where increasing increments of 0% (1 d), 2% (2 d), and 4% (2 d) EtOH was used. After acclimation, EtOH-fed mice were provided 5% EtOH diet for 10 d followed by a 5 g/kg EtOH binge on the final day. Pair-fed (control) mice abided by the same daily feeding regimen; however, a 0% EtOH isocaloric diet was used to match the EtOH-fed mice, where maltose dextrin was used in place of EtOH. EtOH- (catalog: F1258SP) and pair-fed (catalog: F1259SP) diets were made fresh daily and were purchased from Bio-Serv and stored at 4°C until use. Mice were then humanely euthanized with ketamine/xylazine (120/16 mg/kg) followed by exsanguination and tissue collection. In addition, only male mice were used to expand on our existing model and to establish baseline alterations in our omics approaches. This study certainly needs to be repeated with female mice incorporated because there are likely sexually dimorphic responses.

In the current study, we used six liver tissues from each of our four groups (pair-fed+veh., pair-fed+PCB126, EtOH+veh., and EtOH+PCB126), prioritizing highest quality RNA in terms of optical density ratios (260/280; 260/230) and RNA Integrity Number (RIN). For simplicity, we will refer to all group comparisons as follows: *a*) pair-fed+veh. vs. pair-fed+PCB126 as PF(Veh. vs. PCB126); *b*) pair-fed+veh. vs. EtOH+veh. as Veh.(PF vs. EF); *c*) pair-fed+PCB126 vs. EtOH+PCB126as PCB126(PF vs. EF); and *d*) EtOH+veh. vs. EtOH+PCB126as EF(Veh. vs. PCB126).

RNA-Seq Sample Preparation

At the time of tissue collection, hepatic tissues (~ 100 mg) were immediately homogenized in 1 mL of RNA-STAT60 (catalog: CS-502; Tel-Test Inc.). RNA isolation and purification were performed with the standard phenol-chloroform protocol.[28] Following tissue homogenization, the 1-mL lysate was placed into a new tube containing 200 µL of chloroform and vortexed for 30 s at room temperature. Samples were then centrifuged at $12{,}000 \times g$ for 15 min at 4°C. The top, aqueous RNA-containing phase was removed and added to a new tube containing 500 µL of isopropanol and was frozen overnight at −80°C. The following day, samples were thawed on ice and centrifuged at $12{,}000 \times g$ for 10 min at 4°C. Sample supernatants were removed and placed into new tubes. RNA samples were then washed three times with 75% EtOH followed by centrifugation at $7{,}500 \times g$ for 5 min, dried, and reconstituted in DNase/RNase free water. RNA samples were then treated with DNase, Amplification Grade I, to digest single- and double-stranded DNA species (catalog: 18068015; Invitrogen). This was performed at room temperature where 1 µg of RNA, 1 µL of 10X DNase I reaction buffer, 1 µL DNase I Amplification Grade, and variable amounts of DEPC-treated water up to 10 µL total were added into tubes. After treated samples sat at room temperature for 15 min, DNase I was inactivated by the addition of 1 µL 25 mM EDTA. Samples were then heated for 10 min at 65°C. Finally, RNA samples were treated with RNAClean XP beads at a 1:1 v/v ratio to further purify samples to remove salts, dNTPs, and miscellaneous enzymes that may interfere with sequencing (catalog: A66514; Beckman Coulter Life Sciences). RNA sample concentration and purity was then assessed with a NanoDrop One^{C} [spectrometer purchased from ThermoFisher Scientific (catalog: 701-058112)]. Initial and final quality control measures included assessing RNA concentration with a Qubit 4 fluorometer (catalog: Q32854; Invitrogen) and integrity with an Agilent 2100 Bioanalyzer (catalog: 5067-4626; Agilent Technologies). Bioanalyzer quality assessment were performed according to manufacturer's instructions with the Eukaryote Total RNA 6000 Nano electrophoresis kit (catalog: 5067-1511; Agilent Technologies).

RNA-Seq Library Preparation and Sequencing

RNA-Seq libraries were prepared according to manufacturer's protocols using Illumina's TruSeq Stranded reference guide (document: 100000040498 v00; Illumina). Each sample consisted of 300 ng of RNA that was used for poly A enrichment. First and second strand cDNA synthesis was completed using the low sample (LS) portion of the overarching protocol followed by adapter and single-index ligation according to manufacturer's instructions. mRNA libraries were prepared with Illumina's stranded mRNA prep ligation for 96 samples (catalog: 20040534; Illumina). Amplification of cDNA was performed according to the manufacturer's protocol. No deviations from this protocol were made during the preparation of this study's samples. Library concentrations were assessed using a Qubit 4 fluorometer with dsRNA high sensitivity kit (catalog: Q33231; ThermoFisher).

Library size and fragment analysis was assessed on Agilent 4159 Tapestation System on a D5000 screen tape (catalog: 5067-5588; Agilent). Next, individual samples were normalized to 10 nM prior to pooling and then quantified by Qubit analysis. Pooled libraries and PhiX control were diluted and loaded at 1,000 pM with 4% PhiX spiked in. Sequencing was performed on Illumina's NextSeq 2000 platform using a P3 100 cycle reagent kit and P3 flow cell. Libraries were then sequenced with a single 101 cycle read length with two indexes of 8 bp each. FASTQ files were generated with BaseSpace DRAGEN analysis (version 1.2.1). Reads were aligned to the *Mus musculus* mm39 reference genome using STAR (version 2.6).[29] Alignment rates for each sample were in a range of 93.46% to 98.17%. Raw gene counts were determined using HTSEQ-count (version 0.10.0)[30] using the Ensembl GRCm39 (version 106) gene annotations. Raw RNA-Seq data for each sample are available on the Gene Expression Omnibus (GEO) database identified as accession: GSE244388.

Phosphoproteome Tissue Preparation

Liver tissues were harvested during euthanasia and tissue collection, snap frozen in liquid nitrogen, and then were archived in a −80°C freezer. For phosphoproteome analysis, six random liver tissues were used from each of our four groups ($n = 24$). Tissues were removed from the −80°C freezer and weighed and then immediately placed in 2% sodium dodecyl sulfate (SDS) radioimmunoprecipitation (RIPA) buffer containing 10 µL HALT protease and phosphatase inhibitors per mL of RIPA used (catalog: 78443; ThermoFisher Scientific). Tissues were then homogenized in this solution, followed by rocking at 4°C for 30 min. Sample lysates were then centrifuged at 13,000 × *g* for 30 min at 4°C. Supernatant was collected and protein concentrations were measured by bicinchoninic acid (BCA) protein assay, following manufacturer's protocol (catalog: 23225; ThermoFisher Scientific). Lysates were then normalized to 400 µg protein for phosphopeptide preparation.

Phosphopeptide Sample Preparation

Protein lysates were trypsinized at a 1:20 (enzyme:sample) ratio and prepared following ProtiFi's S-Trap mini spin column digestion protocol (website: https://files.protifi.com/protocols/s-trap-mini-long-4-1.pdf; ProtiFi). Phosphopeptides were enriched with MagReSyn's titanium ion-immobilized metal affinity chromatography (Ti-IMAC) microparticles following ReSyn Biosciences MagReSyn's Ti-IMAC protocol.[31] Samples were then purified using C18 PROTO 300 angstrom Ultra MicroSpin columns. Eluate was frozen at −80°C and then dried under a SpeedVac. Dried eluate residue was then stored at −80°C prior to peptide concentration assessment.

Liquid Chromatography (LC) for Phosphopeptide Separation

Samples were diluted to 0.05 µg/µL with 2% (v/v) acetonitrile and 0.1% (v/v) formic acid, and 4 µL were used for LC. Columns used were a 75 µm × 15 cm, 3 µm, 100 angstrom PepMap RSLC C18 EASY-spray separating column at 40°C and a 300 µm × 5 mm, 5 µm PepMap Neo C18 trap cartridge at 30°C (ThermoFisher Scientific). A Dionex Ultimate3000 RSLC nano system was used with solvents A, 0.1% (v/v) formic acid in LC-MS–grade water, and B, 0.1% formic acid in liquid chromatography-mass spectrometry (LC-MS)–grade acetonitrile. Separation was achieved at 200 nL/min with a 5-min linear gradient from 5% solvent B to 7.5% solvent B followed by a 90-min linear gradient from 7.5% solvent B to 35% solvent B. An EASY-Spray source was used to position the separating column emitter 1 mm from the ion transfer capillary of the mass spectrometer (MS), which was set to 320°C and 1.8 kV.

MS for Phosphoproteome

After liquid chromatography separation, an Orbitrap Exploris 480 mass spectrometer was used to analyze eluate. Full MS–ddMS2 method with a 3-s cycle time was generated in Xcalibur (version 4.5.445.18) operating in positive polarity (ThermoFisher Scientific). Scan event 1 of this method attained an MS1 scan for 60,000 resolution, normalized AGC target of 100%, for a scan range of 350–1,400 m/z. Scan event 2 obtained dd-MS2 scans for 7,500 resolution and normalized AGC target of 50% on ions with charged states from 2–6 and a minimum intensity of 8,000 until cycle time completion.

Raw LCMS Data Curation and Analysis

RAW data files were separately searched in PeaksXpro (Bioinformatics Solutions Inc.), using Denovo, PeaksDB, and PeaksPTM algorithms against the UniprotKB *Mus musculus* canonical protein sequences (proteomics ID: UP000000589) downloaded 17 March 2023. Initially, specified enzyme was semispecific trypsin with Carbamidomethyl set as a fixed modification and Oxidation and Phosphorylation as variable modifications. Fragment tolerance was 0.02 Da, and parent tolerance was 15 ppm. A label-free quantification algorithm was then used with PeaksPTM results using a mass error tolerance of 10 ppm and retention time shift tolerance of 6-min. Peptides were accepted at a 1% false discovery rate (FDR) threshold for consideration by the label-free quantification algorithm. A peptide.csv file was exported from this algorithm for data maintenance and curation in Microsoft Excel. One sample part of the EtOH+PCB126 group (EF_PCB3) had a spectral total ion current (TIC) percent coefficient of variation of 35.4%, which is higher than the established cutoff of 10% and was therefore determined to be an outlier. This sample was removed from our downstream analyses and was not included in this study. Raw phosphopeptide data files were uploaded to the online repository MassIVE with identifying code: MSV000093903.

Computational Downstream Analyses

RNA sample fragments per kilobase transcript per million mapped reads (FPKM) values were uploaded to web-based interface MetaboAnalyst (version 5.0) tool. One-factor statistical analysis was used where data were filtered by interquartile range (IQR) and normalized based on group median. RNA-Seq datasets were also uploaded to MetaCore–Integrated pathway analysis for multiomics data software (Clarivate). Data were analyzed with MetaCore for network building and pathway analysis where only processes with a FDR ≤ 0.05 were accepted.

Phosphopeptide mass spectral readouts (peptide area) were normalized by TIC. Phosphopeptide data were then quantile normalized and removed if >40% of the values were missing. For each phosphopeptide, mean and standard deviation (SD) was calculated. A one-way analysis of variance (ANOVA) was used to test phosphopeptide significance between different groups. After *p*-values were generated, *p*-values were adjusted (adjusted *p*-value; *q*-value) by using the Benjamini-Hochberg method to control for FDR. Phosphopeptide data were then uploaded to the web-based interface MetaboAnalyst (version 5.0) R tool. Remaining missing values were replaced by the limit of detection (1/5 of minimum positive value of each variable). One-factor statistical analysis was used where data was filtered by IQR and normalized based on group median.

Real-Time PCR Analyses

Liver tissues were homogenized in RNA-STAT60 (catalog: CS-502; Tel-Test Inc.), and total RNA was extracted by the method described above in the "RNA-Seq Sample Preparation" section. RNA concentration and purity was examined with a NanoDrop One^{C} spectrometer (catalog: 701-058112; ThermoFisher). cDNA was reverse transcribed from 3 μg RNA to produce cDNA with QScript, a single-step cDNA synthesis reagent (catalog: 95048-500; Quantabio). Real-time polymerase chain reaction (RT-PCR) was performed on a CFX384 Real-Time platform (Bio-Rad). The RT-PCR program occurred for 39 cycles, where one cycle consists of 2 mins at 95°C, 5 s at 95°C, and then 30 s at 60°C. iTaq Universal Probe Supermix was employed during experiment setup (catalog: 1725134; Bio-Rad). Relative mRNA expression was calculated using the $2^{-\Delta\Delta Ct}$ method with Glyceraldehyde-3-Phosphate Dehydrogenase (GAPDH) as the housekeeping gene for liver tissues (catalog: 4351309; Applied Biosystems). Fold induction was normalized to the control group, pair-fed+veh., and was set to a value of "1." TaqMan probes were purchased from ThermoFisher Scientific, and the following list contains probe names and their respective assay IDs: *Abcb10* (Mm 00497926_m1), *Slc46a3* (Mm00503612_m1), *Tuba8* (Mm01184204_m1), and *Ugt1a6b* (Mm07308190_s1).

Western Blot Analysis

Approximately 50–100 mg mouse liver tissue was homogenized in RIPA Buffer (100 mg tissue/0.5 mL RIPA). A HALT protease and phosphatase inhibitor cocktail was added to this tissue lysate at 10 μL/mL of RIPA buffer used (catalog: 78443; ThermoFisher Scientific). Whole protein concentration was assessed by BCA protein assay, following manufacturer's protocol (catalog: 23225; ThermoFisher Scientific). Normalized 50 μg protein was loaded and separated on 4%–15% Mini-PROTEAN TGX Stain-Free gels (catalog: 4568086; Bio-Rad). A total of six protein lysates per group ($n = 24$) were used, where two sets of three protein lysates per group were loaded onto two different gels in a representative fashion to account for possible running and antibody incubation differences. Separated proteins were then transferred to polyvinylidene difluoride membranes (catalog: IPVH00010; Millipore Sigma), blocked (catalog: 1706404; Bio-Rad), and incubated with primary and secondary antibodies. Primary rabbit monoclonal antibodies, phospho-Janus kinase 2 (p-JAK2) (catalog: 3776S), Janus kinase (JAK2) (catalog: 3230S), phospho-signal transducer and activator of transcription 5 (p-STAT5) (catalog: 9359S), signal transducer and activator of transcription 5 (STAT5) (catalog: 94205S), progesterone receptor membrane component 1 (PGRMC1) (catalog: 13856T), and β-Actin (catalog: 8457S), were purchased from Cell Signaling Technologies. Primary antibodies p-JAK2, JAK2, p-STAT5, and STAT5 were diluted 1:1,000 with 5% bovine serum albumin (BSA) in tris-buffered saline containing 0.1% Tween-20 (TBS-T). Primary antibody control β-Actin was diluted to 1:2,000 with 5% BSA in TBS-T. Primary antibodies were applied to membranes overnight at 4°C. Donkey anti-rabbit secondary antibody was purchased from Jackson ImmunoResearch Laboratories Inc. (catalog: 711-035-152) and was diluted to 1:2,000 in 5% milk-fat TBS-T for 1 h at room temperature. Phosphoproteins were probed first, followed by stripping buffer (catalog: 46430; ThermoFisher Scientific) for 15 min at room temperature to cleave bound antibodies. Primary antibodies for the protein corresponding to the phosphoprotein were then probed on the same membrane overnight and analyzed the next day. After probing for the phosphoprotein and protein, the same membrane was finally used to probe for housekeeping control, β-Actin. The ladder control for protein molecular weight identification was Bio-Rad's Precision Plus Standard Kaleidoscope (catalog: 1610375). Western blot band visualization was performed with Bio-Rad's ChemiDoc station on the chemiluminescent setting for protein bands and on colorimetric setting for ladder control detection.

Metals Analysis

Approximately 50 mg of liver tissue were digested in 800 μL of 70% nitric acid (catalog: A509-P500; ThermoFisher Scientific) and 200 μL of hydrogen peroxide (catalog: 95321; Millipore Sigma) for 4 h at 85°C. Sample homogenates were then cooled to room temperature and diluted to a final concentration of 5% nitric acid with MilliQ DI water. Samples were then filtered by 45 μm filter.

Metal quantification was performed using Agilent 7800 inductively coupled plasma mass spectrometry (ICP-MS) (Agilent Technologies). This Agilent ICP-MS was optimized with 1 ppb tuning solution, and the assay program was tuned by 10 ppb turning solution (catalog: 5188-6564; Agilent Technologies). An autosampler SPS 4 was used to load samples. Twenty-five metals calibration standards were purchased from Inorganic Ventures (catalog: IV-STOCK-50), and serial metal standard dilutions were made with the same acid matrix of samples. Internal standards used were purchased from Agilent (catalog: 5188-6525) and were mixed with each sample for calibration. Assay program was run on Agilent MassHunter software with helium mode and each sample was read three times for a final mean value. Metals that were measured include sodium (Na), potassium (K), magnesium (Mg), calcium (Ca), Iron (Fe), manganese (Mn), cobalt (Co), copper (Cu), zinc (Zn), molybdenum (Mo), and selenium (Se). The limit of detection for each metal are as follows: Na = 3.50 ng/mL; K = 4.52 ng/mL; Mg = 0.170 ng/mL; Ca = 27.6 ng/mL; Fe = 0.059 ng/mL; Mn = 0.012 ng/mL; Co = 0.002 ng/mL; Cu = 0.014 ng/mL; Zn = 0.591 ng/mL; Mo = 0.003 ng/mL; Se = 0.437 ng/mL.

Statistical Analyses

Sequenced read quality was assessed using FastQC (version 0.10.1) for each run.[32] Sequences were of good quality, and trimming was not necessary. Raw counts were then normalized using the relative log expression method and filtered to exclude genes with fewer than 10 counts across all samples. Differential expression analysis was performed using DESeq2.[33] DESeq2 was executed in the R programing environment, using a negative binomial regression model to analyze pairwise comparison. Statistical significance was determined by *q*-values ≤0.05. GO biological processes were generated by the R package clusterProfiler for sets of DEGs in each group comparison.

All statistical analyses were performed with GraphPad Prism (version 9.5.1; GraphPad Software Inc.) for Windows, using a two-way ANOVA, unless otherwise noted. Two-way ANOVA was performed where our two factors were diet (pair-fed vs.

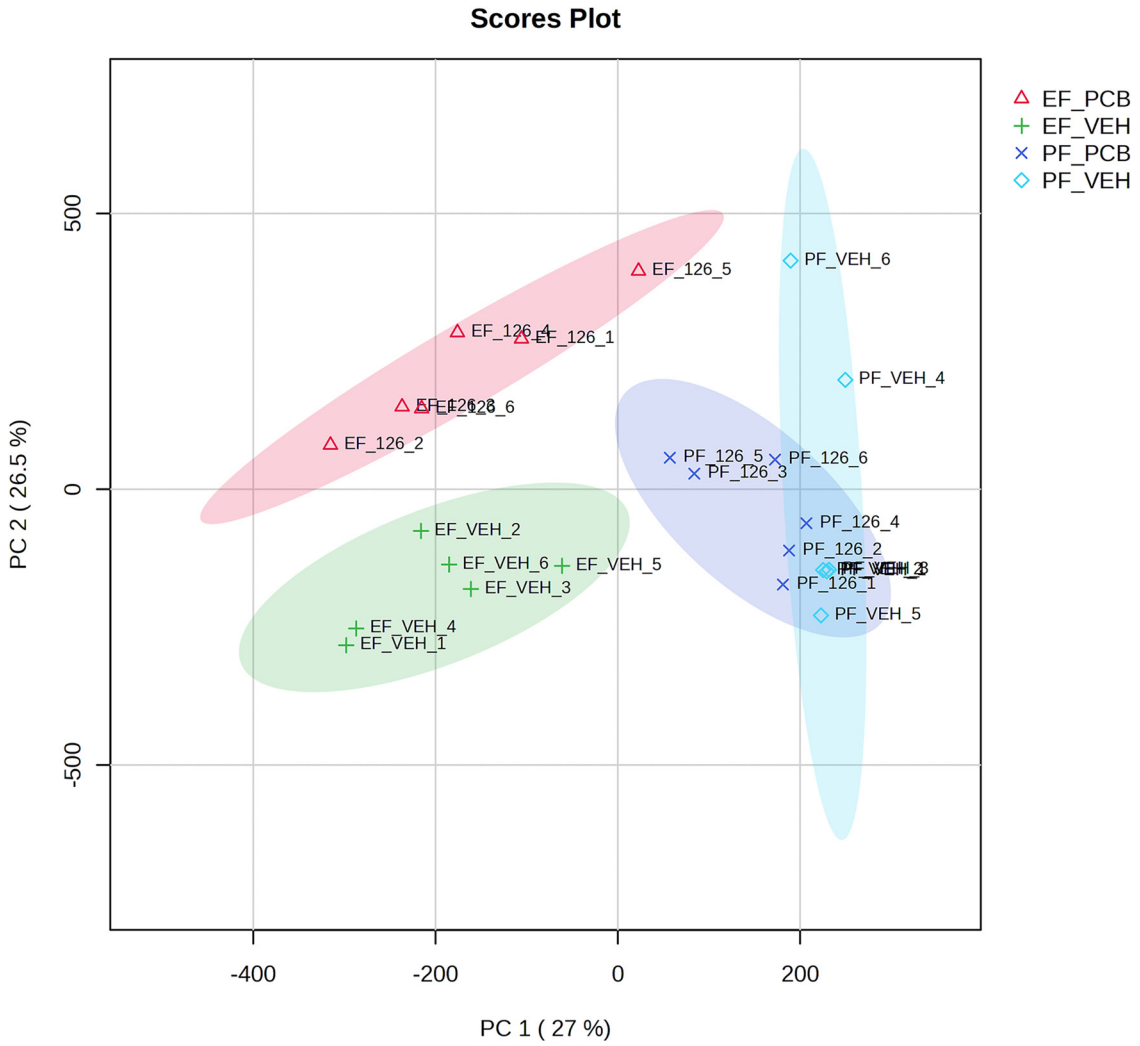

Figure 1. PCA for all samples ($n = 6$; $n = 24$). PCA plot was generated on MetaboAnalyst based on FPKM values, filtered by interquartile range, and normalized based on group median. Individual samples are identified by diet_exposure_number, where diet is either PF or EF, and exposure is either vehicle (VEH) or PCB126 (PCB). Note: EF, EtOH-fed; FPKM, fragments per kilobase per million mapped fragments; PC, principal component; PCA, principal component analysis; PF, pair-fed.

EtOH-fed) and exposure (vehicle vs. PCB126). Significance was determined with an alpha level set to 0.05. Tukey's post hoc test was used to compare different groups for multiple comparisons. Western blot band volume intensity was measured by Bio-Rad's Image Lab software (version 6.1.0 build 7). After background subtraction, proteins of interest band intensity were divided by their respective β-Actin band intensity for each sample/column. The ratio of phosphoprotein:protein was determined after individually dividing each phosphoprotein and protein by their respective β-Actin band/column. Please refer to Supplemental Excel file S1 to view summary data or some descriptive statistics for figures generated in this work.

Results

Description of the Hepatic Transcriptome

We first examined group transcriptome variance caused by EtOH feeding or PCB126 exposure by principal component analysis (PCA) generated on MetaboAnalyst (Figure 1). The two-dimensional PCA plot demonstrates that pair-fed mice exposed to PCB126 were slightly varied in comparison with pair-fed+veh. EtOH feeding overall was the major source of variation where EtOH+veh. and EtOH+PCB126 were two unique populations relative to pair-fed controls. An interesting finding was that we observed variance between PCB126- and pair-fed mice; however, there was a large degree of variance between the EtOH+veh. vs. EtOH+PCB126. Relative to controls, mice exposed to PCB126 exhibited a distinct transcriptome landscape within EtOH-fed mice.

Table 1 displays the total DEG count and breaks it down into those genes that were expressed at a higher or lower level in comparison with control for all group comparisons. Pair-fed vs. EtOH-fed mice (regardless of exposure) had a total of 5,919 DEGs, where 2,834 were expressed at a higher level and 3,085 were expressed at a lower level. Vehicle- vs. PCB126-exposed mice (regardless of diet) had a total of 449 DEGs, where 278 were higher and 171 were lower. Regarding total DEGs, the PF(Veh. vs. PCB126) comparison had 503 DEGs; the Veh.(PF vs. EF) comparison had 4,474 DEGs; the PCB126(PF vs. EF) comparison had 4,832 DEGs; and the EF(Veh. vs. PCB126) comparison had 907 DEGs. Of the up-regulated DEG set, the PF(Veh. vs. PCB126) comparison had 339 DEGs; the Veh.(PF vs. EF) comparison had 2,231 DEGs; the PCB126(PF vs. EF) comparison had 2,214 DEGs; and the EF(Veh. vs. PCB126) comparison had 536 DEGs. Of the down-regulated DEG set, the PF(Veh. vs. PCB126) comparison had 164 DEGs; the

Table 1. Count of significant DEGs for each group comparison for the total, up-regulated, and down-regulated DEGs where pair-fed and/or vehicle groups are controls relative to EtOH-fed and/or PCB126 groups.

	DEGs ($p \le 0.05$; $q \le 0.05$; $\lvert \log 2FC \rvert \ge 0$; FPKM ≥ 1 in ≥ 3 samples; average FPKM ≥ 1)		
Group comparison	Total	Inc.	Dec.
Pair-fed vs. EtOH-fed	5,919	2,834	3,085
Veh. vs. PCB126	449	278	171
Veh.(Pair-fed vs. EtOH-fed)	4,474	2,231	2,243
PCB126(Pair-fed vs. EtOH-fed)	4,832	2,214	2,618
PF(Veh. vs. PCB126)	503	339	164
EF(Veh. vs. PCB126)	907	536	371

Note: Significance was determined by DESeq2 where DEGs were accepted for $q \le 0.05$, $p \le 0.05$, $\lvert \log 2FC \rvert \ge 0$, FPKM ≥ 1 in ≥ 3 samples, and average FPKM ≥ 1. Pair-fed vs. EtOH-fed ($n = 12$ vs. 12); Veh. vs. PCB126 ($n = 12$ vs. 12); Veh.(Pair-fed vs. EtOH-fed) ($n = 6$ vs. 6); PCB126(Pair-fed vs. EtOH-fed) ($n = 6$ vs. 6); Pair-fed(Veh. vs. PCB126) ($n = 6$ vs. 6); EtOH-fed(Veh. vs. PCB126) ($n = 6$ vs. 6). Dec., decreasing; DEGs, differentially expressed genes; EF, EtOH-fed; FC, fold change; FPKM, fragments per kilobase per million mapped fragments; Inc., increasing; PF, pair-fed; Veh., vehicle.

Veh.(PF vs. EF) comparison had 2,243 DEGs; the PCB126(PF vs. EF) comparison had 2,618 DEGs; and the EF(Veh. vs. PCB126) comparison had 371 DEGs.

We also evaluated the top 20 DEGs with the lowest q-values in the EF(Veh. vs. PCB126) group, where a total of 907 significant DEGs were observed. The top 20 up- and down-regulated DEGs with the lowest q-values are listed in Table 2. In the up-regulated gene set, cytochrome P450 family 1 subfamily A member 1 and 2 (*Cyp1a1*, *Cyp1a2*) had the lowest q-values in comparison with all other genes and are canonical AhR targets. An interesting finding was that *Cyp1a1* expression was significantly $\sim$4-fold higher due to EtOH feeding in the Veh.(PF vs. EF) comparison (Figure S4). Other genes noted in the up-regulated gene set include muscle isoform of pyruvate kinase (*Pkm*), glutathione peroxidase (*Gpx2*), monoamine oxidase A (*Maoa*), and transforming growth factor beta 2 (*Tgfβ2*). In the down-regulated gene set, UDP glucuronosyltransferase family 1 member A6b (*Ugt1a6b*) had the lowest q-value. Other interesting, down-regulated genes of note include perilipin 4 (*Plin4*), canonical PXR target cytochrome P450 family 3 subfamily A member 11 (*Cyp3a11*), and lactate dehydrogenase A (*Ldha*).

Four specific genes were chosen from the top 20 DEGs with the lowest q-values in the EF(Veh. vs. PCB126) comparison for validation by RT-PCR (Figure S1). These genes were specifically chosen based on differing effects from EtOH and/or PCB126 (e.g., up-regulation by PCB126 only). Figure S1 displays gene expression of ATP binding cassette subfamily B member 10 (*Abcb10*), UDP glucuronosyltransferase 1 family, polypeptide A6B (*Ugt1a6b*), solute carrier family 46, member 3 (*Slc46a3*), and Tubulin, alpha 8 (*Tuba8*). *Abcb10* is a multidrug resistant mitochondrial transporter, and its expression was found to be down-regulated $\sim$50% by EtOH feeding (Figure S1A). *Ugt1a6b* is a phase II enzyme part of the glucuronidation process, and its expression was slightly higher following PCB126 exposure in pair-fed mice. It is interesting to note that we observed a significant interaction effect, where PCB126 exposure in EtOH-fed mice led to down-regulation of *Ugt1a6b*'s expression $\sim$60% (Figure S1B). *Slc46a3* is a lysosomal transporter involved in the distribution of small molecules and catabolites,[34] and its expression was found to be 10-fold higher in PCB126-exposed pair-fed mice. We noted an interaction effect in EtOH-fed mice, where PCB126's induction of *Slc46a3* was mitigated to $\sim$ 5-fold, likely because of ethanol feeding (Figure S1C). Finally, *Tuba8*, a noncanonical alpha-tubulin molecule involved in microtubule formation and signaling,[35] was up-regulated 25-fold in pair-fed mice following PCB126 exposure relative to vehicle-exposed mice; however, our analyses indicated a significant interaction where *Tuba8* was up-regulated 60-fold in PCB126-exposed, EtOH-fed mice (Figure S1D) relative to pair-fed, vehicle-exposed mice.

Enriched GO Processes

We examined enriched GO biological processes via the clusterProfiler R package to gather connections between gene expression/products and reported biological observations. Figure 2 displays the top 20 significantly enriched GO biological processes for the EF(Veh. vs. PCB126) comparison where 907 genes were significantly different within this comparison; Figure 2 is sorted by lowest q-value (p.adjust). The top annotated term in this list was "peptidyl-tyrosine modifications." An interesting aspect is that the third, fifth, and sixth annotated enriched GO terms were also related to this top (smallest q-value) term and are listed

Table 2. Top 20 most significant up- and down-regulated DEGs in the EF(Veh. vs. PCB126) comparison ($n = 6$ vs. 6), sorted by lowest q-value.

Up-regulated DEGs			Down-regulated DEGs		
Gene	Log_2FC	q-value	Gene	Log_2FC	q-value
Cyp1a1	8.64	3.024×10^{-214}	*Ugt1a6b*	−1.01	1.047×10^{-18}
Cyp1a2	3.63	1.868×10^{-106}	*Plin4*	−1.76	1.416×10^{-11}
Slc46a3	2.55	9.043×10^{-64}	*Cyp3a11*	−1.26	3.332×10^{-9}
Cyfip2	3.51	1.862×10^{-42}	*Cyp2d40*	−0.88	6.118×10^{-9}
Ugt1a9	2.15	9.988×10^{-40}	*Alas2*	−0.86	7.045×10^{-9}
Pkm	1.99	2.193×10^{-35}	*Rnf169*	−0.48	2.589×10^{-8}
Htatip2	1.59	1.062×10^{-34}	*Fam210b*	−0.53	1.022×10^{-7}
Gpx2	3.95	5.982×10^{-33}	*Paqr9*	−0.85	1.520×10^{-7}
Maoa	1.55	5.295×10^{-30}	*1810055G02Rik*	−0.81	1.771×10^{-7}
Aldh3b1	2.06	1.256×10^{-25}	*Apoa1*	−1.02	2.401×10^{-7}
Pcp4l1	2.19	2.778×10^{-23}	*St3gal3*	−0.58	4.108×10^{-7}
Rtn4rl2	2.91	3.684×10^{-23}	*Nrbp2*	−0.70	5.114×10^{-7}
Tuba8	1.55	1.246×10^{-21}	*Elovl2*	−0.63	6.476×10^{-7}
Selenbp1	1.31	3.062×10^{-21}	*Smarcc2*	−0.35	1.048×10^{-6}
Coro6	2.20	1.624×10^{-16}	*Ulk1*	−0.64	1.281×10^{-6}
Cyp1b1	2.99	1.485×10^{-15}	*Serpina11*	−0.75	1.658×10^{-6}
Insl6	2.26	4.771×10^{-14}	*Zfp865*	−0.46	1.959×10^{-6}
Nqo1	1.49	3.449×10^{-13}	*Ldha*	−0.68	4.258×10^{-6}
Tmem86b	1.07	4.125×10^{-12}	*Scp2*	−0.49	1.284×10^{-5}
Tgfb2	2.50	1.416×10^{-11}	*Gm50136*	−1.14	1.469×10^{-5}

Note: Significance was determined by DESeq2, where DEGs were accepted for $q \le 0.05$, $p \le 0.05$, $\lvert \log 2FC \rvert \ge 0$, FPKM ≥ 1in ≥ 3 samples, and average FPKM ≥ 1. Difference is relative to the control group (EtOH+veh.). DEGs, differentially expressed genes; FC, fold change; FPKM, fragments per kilobase per million mapped fragments.

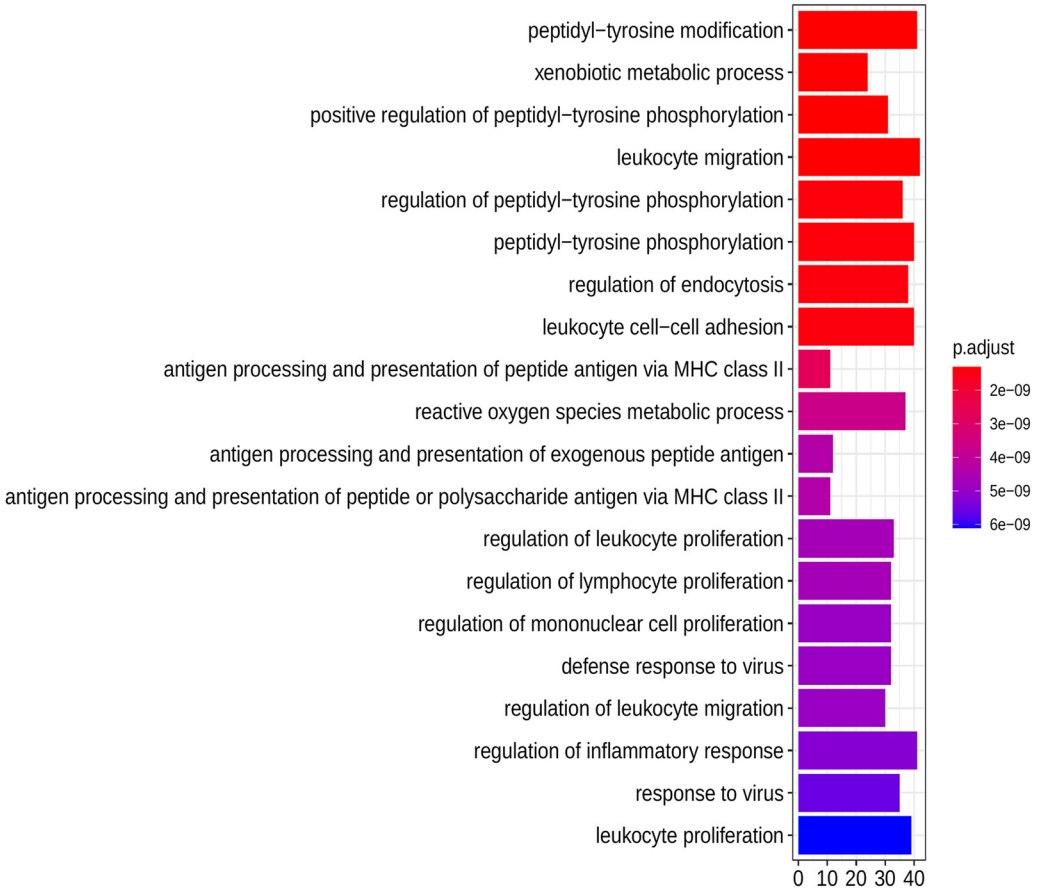

Figure 2. Top 20 significantly enriched GO biological processes of the EF(Veh. vs. PCB126) comparison ($n = 6$ vs. 6), sorted by lowest adjusted p-value (p.adjust). GO biological processes were determined by R package clusterProfiler, where DESeq2 differential expression analysis results were implemented for this pairwise comparison. Please refer to the Supplemental Excel file for summary data for this figure. Note: EF, EtOH-fed; GO, gene ontology; p.adjust, adjusted p-value.

as positive regulation of peptidyl-tyrosine phosphorylation, regulation of peptidyl-tyrosine phosphorylation, and peptidyl-tyrosine phosphorylation, respectively. Other annotated terms within this comparison included xenobiotic metabolic process, regulation of endocytosis, or those related to immune cell regulation. We hypothesized that phosphorylation, particularly of tyrosine residues, may be impacted by this exposure paradigm to disrupt signaling or other catalytic functions by phosphorylation.

We also examined the top 25 significantly enriched GO molecular function processes in MetaCore to identify connections between gene expression and reported molecular function observations. Figure 3 displays the top 25 significantly enriched GO molecular functions from the 907 genes that were significant in the EF (Veh. vs. PCB126) comparison and is sorted by lowest adjusted q-value (p.adjust) and decreasing signal. The top (lowest p-value) annotated term in this list was "binding," followed by "protein binding." We found it curious that several other related, significant terms were observed in this list, including "ion binding," "cation binding," "metal ion binding," "transition metal ion binding," and "zinc ion binding." We hypothesize that metal binding, particularly Zn binding, may be lower in EtOH+PCB126 mice relative to EtOH+veh. mice.

Description of the Hepatic Phosphoproteome

To follow up on the identified GO biological process, "peptidyl tyrosine modifications," we performed quantitative, label-free phosphoproteomics to interrogate differences between group phosphoproteomes. Figure 4A displays a PCA plot to describe the variance among all groups. It was observed that SD areas of the pair-fed groups overlap considerably, whereas there was some variation in EtOH-fed mice. Little variance was observed by PCB126 exposure in both dietary groups, especially in pair-fed mice. Slightly more variance was observed by PCB126 exposure in the EtOH-fed mice. One sample in the EtOH+PCB126 group (EF_PCB1) deviated more than all other samples but was not considered an outlier based on mass spectral traces. Four of the top six GO biological processes from the RNA-Seq dataset sorted by lowest q-value (p.adjust) contained descriptions of peptidyl-tyrosine modification/phosphorylation (Figure 2). Therefore, we quantified the relative differences of phosphorylated tyrosine in the phosphoproteome dataset and found no significant differences in phosphorylated tyrosine among all groups (Figure 4B). There were also no significant differences among groups when evaluating all other amino acid residues that are capable of being phosphorylated or the sum of phosphorylated amino acids.

Because of this discrepancy, we generated a network on MetaCore specifically around the term "peptidyl-tyrosine modifications" for the EF(Veh. vs. PCB126) comparison (Figure S2). We observed differential expression in genes involving the Janus Kinase–Signal Transducer and Activator of Transcription (JAK-STAT) pathway, where tyrosine phosphorylation is particularly required for proper signal transduction.[36] Therefore, we evaluated how this exposure paradigm may have altered the phosphorylation of these two critical proteins. Figure S3 displays quantitative bar graphs of phospho- (p-) JAK2, JAK2, p-STAT5, and STAT5

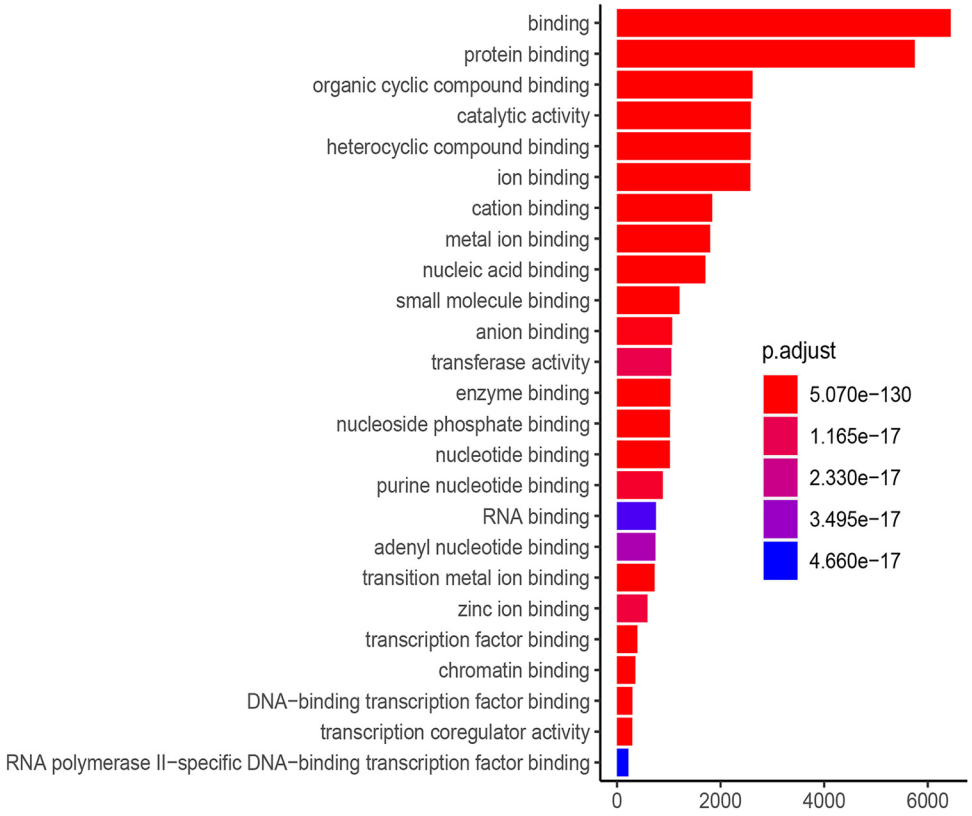

Figure 3. Top 25 significantly enriched GO molecular functions of the EF(Veh. vs. PCB126) comparison ($n = 6$ vs. 6), sorted by lowest adjusted p-value (p.adjust) and decreasing signal. Enriched GO molecular functions were determined on the MetaCore platform for the EF(Veh. vs. PCB126) dataset for a false discovery rate set at 0.05. Please refer to the Supplemental Excel file for summary data for this figure. Note: EF, EtOH-fed; GO, gene ontology; p.adjust, adjusted p-value.

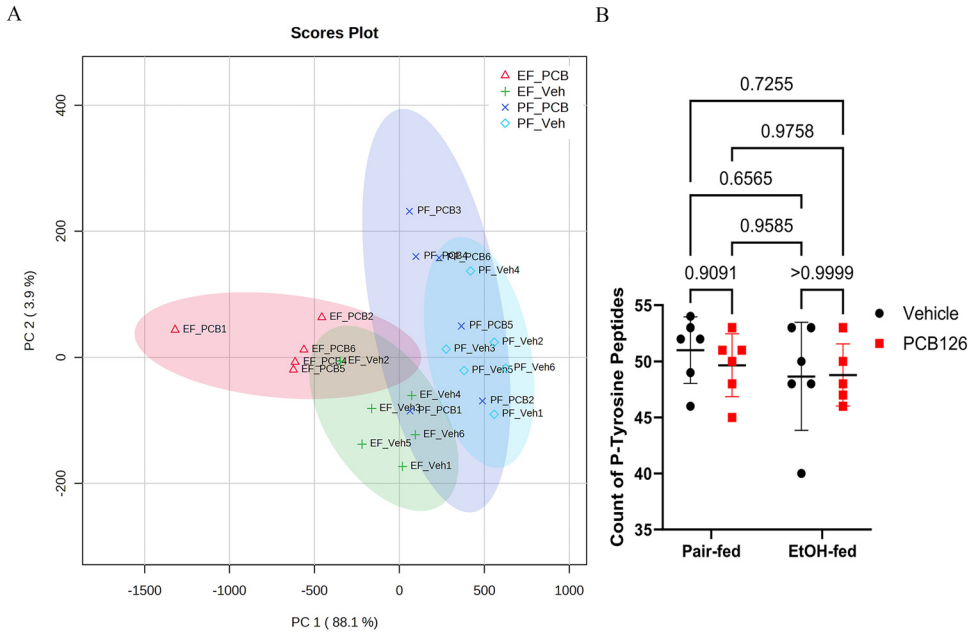

Figure 4. Characterization of phosphoproteome dataset for all samples, excluding outlier EF_PCB3 ($n = 23$). (A) PCA of each group where SD areas encircle each sample. PCA plot was generated on MetaboAnalyst where phospho-peptides were quantile normalized and then removed if >40% of the values were missing. Missing values were replaced by the limit of detection (1/5 of minimum positive value of each variable). (B) Total count of phosphorylated tyrosine for each sample. All peptides containing a phosphorylated tyrosine residue were counted if the peptide area was >0. Values are represented as mean ± SD with an alpha level set to 0.05. Significance was determined by two-way ANOVA and Tukey's post hoc test, where post hoc p-values are provided above the figure. Please refer to the Supplemental Excel file for summary data for this figure. Note: ANOVA, analysis of variance; EF, EtOH-fed; PC, principal component; PCA, principal component analysis; PF, pair-fed; SD, standard deviation; Veh, vehicle.

and their representative western blot images. Two-way ANOVA analyses indicated that a main effect was observed for all p-proteins and proteins were significantly lower in EtOH-fed mice, except for p-JAK2/JAK2 ratio. Tukey's post hoc test revealed only significant EtOH effects where p-JAK2 and JAK2 were lower only in PCB126 exposed group comparisons. However, a significant interaction effect was observed for p-JAK2 where the EtOH+PCB126 group had the lowest mean abundance, relative to EtOH+veh. and pair-fed controls. p-JAK2/JAK2 protein ratio was mitigated by PCB126 in EtOH-fed mice; however, this result was not significant and was only normalized to pair-fed group levels. Although there was no significant alteration regarding the total phosphoproteome or tyrosine phosphopeptides, significant differences were observed in other individual phosphopeptides between group comparisons. For example, 20 phosphopeptides were significantly different in the EF(Veh. vs. PCB126) comparison (Excel Table S1). Other significantly different phosphopeptides between-group comparisons are listed in Excel Table S1.

Hepatic Metal Levels and Transcription Factor Activity

MetaCore analyses revealed that several GO molecular function processes contained "ion binding," "metal ion binding," and "zinc ion binding" to be significant and were among the top 25 processes with the lowest *q*-values (p.adjust) (Figure 3). Thus, we measured hepatic metal levels by ICP-MS to assess how these levels differed between exposure paradigms. Figure 5 displays four critical micronutrient metals: (A) Na, (B) Co, (C) Mg, and (D) Zn. A significant interaction effect was observed where sodium was higher in EtOH+veh. mice (1,062.54 μg/g) relative to pair-fed controls; however, this level was normalized to pair-fed levels in EtOH+PCB126 mice (767.34 μg/g). Co, Mg, and Zn were significantly lower in PCB126-exposed ($p = 0.0020$, 0.0019, 0.0069; respectively) and EtOH-fed ($p = 0.0012$, <0.0001, <0.0001; respectively) mice. An important observation was that Co, Mg, and Zn were significantly lower in mean in the EtOH+PCB126 group relative to all other groups. Other metals that were quantified are found in Table S1. All metal levels were significantly impacted by EtOH feeding, and only seven metal levels were significantly impacted by PCB126 exposure.

In addition, we used MetaCore's Transcription Factor Interactome function to analyze transcription factor connectivity for the EF(Veh. vs. PCB126) transcriptome comparison. Table 3 displays the top 20 significant transcription factors (sorted by highest *z*-score) that are involved in the EF(Veh. vs. PCB126) comparison. The highest *z*-score transcription factor in this list was *Fbi1*, also known as zinc finger and BTB domain containing 7A (*Zbtb7a*). Other transcription factors in this list included *Gata1*, *Klf4*, *Hnf4α*, and *Gata2*. An important finding was that 8 of these top 20 significant transcription factors contain zinc-finger domains. We postulate that PCB126 promotes alcohol-induced Zn deficiency and alters zinc-finger transcription factor function, resulting in transcriptional reprogramming and phenotypic changes observed in our prior study.

Discussion

With increasing research providing convincing evidence on the negative impact of environmental pollutants on MASLD, it is pertinent to examine toxicant effects in alcohol-associated liver pathology. The aim of the current study was to generate mechanistic hypotheses by RNA-Seq and to subsequently test these hypotheses. Excessive alcohol consumption has been shown to impact a wealth of molecules such as nucleic acids,[37,38] proteins,[21,37] cofactors,[37] and various micronutrients.[39,40] Thus, it was no major surprise to find that some differences in these molecules that were identified following EtOH exposure, such as Zn, were worsened after PCB126 exposure.

Transcriptome PCA (Figure 1) indicated that the pair-fed+PCB126 group only slightly deviated in terms of variance from the pair-fed+veh. group by increasing along the *y*-axis. This parallels our findings in Table 1, where there were only 503 total DEGs in the PF(Veh. vs. PCB126) comparison. Although this total DEG count is seemingly a high number, it is relatively the smallest change respective to other comparisons and about half in comparison with the EF (Veh. vs. PCB126) group. An important finding was that the EtOH+PCB126 group was completely unique in variance relative to the EtOH+veh. group and had 907 DEGs. The transcriptional differences in PCB126-exposed, EtOH-fed mice in part may explain some of the phenotypes observed in our characterization study. For instance, of the top 20 significant up- and down-regulated DEGs in EF(Veh. vs. PCB126) comparison, up-regulation of solute carrier family 46 member 3 (*Slc46a3*)[34] and down-regulation of progestin and adipoQ receptor family member 9 (*Paqr9*),[41] apolipoprotein A-1 (*Apoa1*),[42] and elongation of very long chain fatty acids protein 2 (*Elovl2*)[43] have demonstrated to be involved in the development of steatosis or altered lipid metabolism.

Two primary hypotheses were generated from this RNA-Seq study to elucidate potential EtOH and PCB126 interaction mechanisms: *a*) phosphorylation of tyrosine residues will be significantly lower in the EtOH+PCB126 group relative to EtOH+veh., and *b*) hepatic metal levels will be significantly lower in EtOH+PCB126 mice relative to EtOH+veh. Based on previous research, the phosphoproteome was expected to be altered by EtOH[21,44] and PCB126 exposure.[22] Phosphoproteome PCA (Figure 4) and p-JAK2/p-STAT5 (Figure S3) western blot analysis demonstrated that EtOH was the primary driver of any phosphorylation differences. PCB126 did not exacerbate these changes, and, therefore, this data led us to rejecting our first hypothesis.

Regarding the top 25 GO molecular functions in the RNA-Seq dataset (sorted by lowest adjusted *p*-value), several processes were revealed to be involved with ion, metal, or Zn binding (Figure 3). A recent epidemiology study inferred that unbalanced metal mixtures can contribute to liver disease status.[45] Our second generated hypothesis stated that metals, particularly Zn, will be significantly lower in the EtOH+PCB126 group relative to controls. Quantified hepatic metals by ICP-MS revealed that Co, Mg, and Zn were significantly lower in the EtOH+PCB126 group relative to the EtOH+veh. group. Malnutrition[46] and inadequate micronutrients[39] are critical factors in ALD pathogenesis. Zn deficiency in rodents has shown to promote reduced hepatic glycogen stores[47] and has also been associated with increased steatosis in humans.[48] Both reduced glycogen and increased steatosis end points were observed in our previous study.[26] Further loss of essential metals by PCB126 in ALD may be an additive effect promoting disease status and limit metal availability for functional purposes, such as in kinases or transcription factors. For example, many vital transcription factors use Zn in zinc finger domains to regulate target gene expression.[49] Zn deficiency or zinc-finger dysfunction is also a well characterized phenomenon that occurs in ALD, where patients are often advised by health care providers to incorporate more Zn in their diet.[50] Zn deficiency has shown to promote alcohol-induced liver injury,[51] whereas Zn supplementation attenuates injury.[52,53] This study demonstrated that Zn was lower in EtOH-fed mice relative to pair-fed controls, and was at lowest levels in the EtOH+PCB126 group (Figure 5; Table S1). Future mechanistic studies are needed to better understand how PCB126 augments EtOH-mediated Zn deficiency. It is postulated that Zn absorption, and thus availability, is significantly impacted in this model, and supplementation would alleviate metabolic abnormalities revealed in our characterization study.[26]

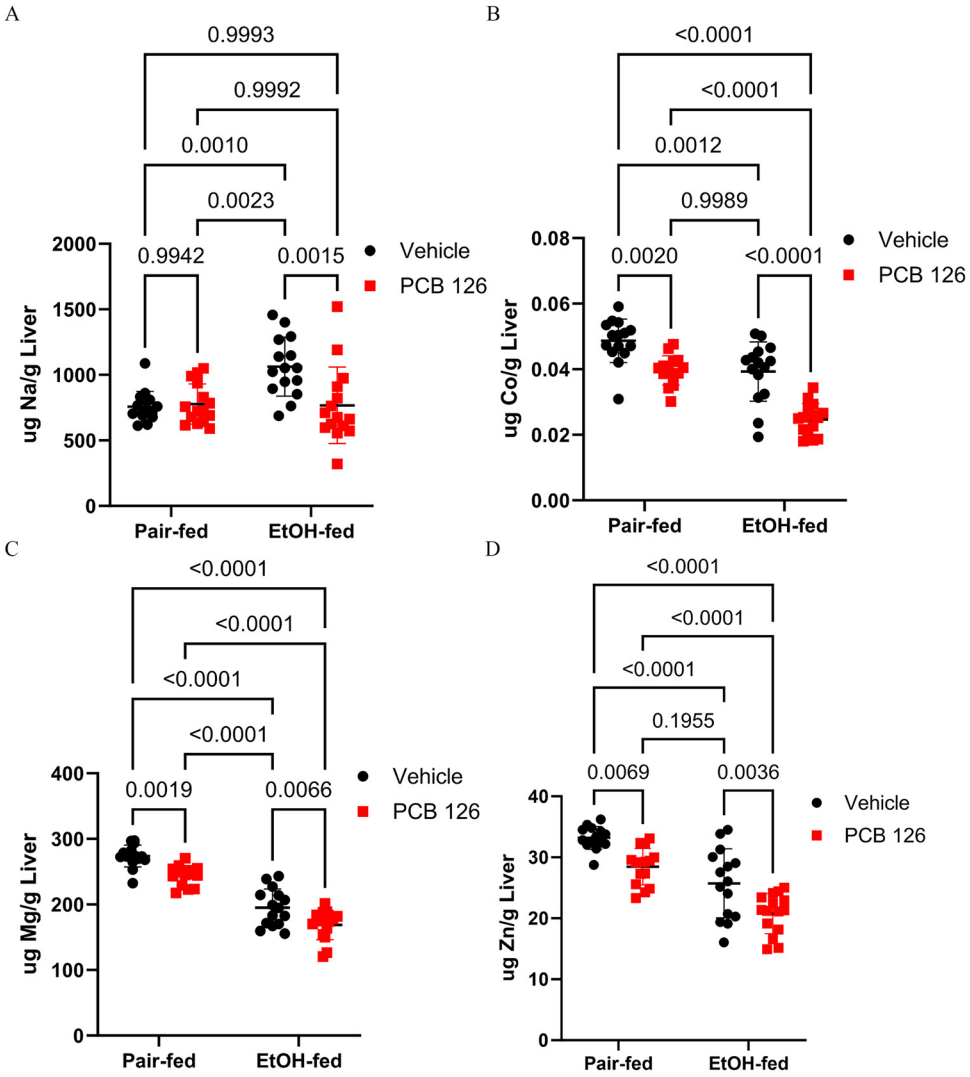

Figure 5. ICP-MS analysis of four essential micronutrient metals: (A) Na; (B) Co; (C) Mg; and (D) Zn. Values are represented as mean ± SD with an alpha level set to 0.05 ($n = 15$; $n = 60$). Significance was determined by two-way ANOVA and Tukey's post hoc test, where post hoc p-values are provided above each graph. Please refer to the Supplemental Excel file for summary data for this figure. Note: ANOVA, analysis of variance; Co, cobalt; ICP-MS, inductively coupled plasma mass spectrometry; Mg, magnesium; Na, sodium; SD, standard deviation; Zn, zinc.

It was revealed that eight of the top 20 significant transcription factors (Table 3) contained zinc-finger domains in this interactome. Each transcription factor was calculated to be overconnected (ratio > 1) in this dataset; however, their activity and ability to use Zn is unknown. Previous cell culture research has shown that Zn deficiency can impact zinc-finger conformation and therefore DNA binding capability and transcription.[54] *Hnf4α* is one transcription factor of interest that contains a zinc-finger domain and is well known for its diverse roles in liver metabolism and pathology.[55,56] The transcription factor interactome analysis revealed that *Hnf4α* was a significant, overconnected (ratio = 1.78) gene in the EF(Veh. vs. PCB126) dataset. In addition, *Hnf4α* has numerous target genes, including albumin (*Alb*), phosphoenolpyruvate kinase 1 (*Pck1*), pyruvate kinase L/R (*Pklr*), and sterol regulatory element binding protein 1 (*Srebf1*). Each of these transcripts were assessed in our characterization study, where relative mean expression levels were the lowest in the EtOH+PCB126 group relative to all other groups.[26] The lower transcription of these target genes suggests reduced *Hnf4α* activity as a consequence of Zn deficiency. In a 12-wk rodent study, Kang et al.[57] demonstrated that although *Hnf4α* expression was unchanged by EtOH feeding, its activity was reduced. Zn supplementation in this study[57] replenished *Hnf4α* activity to control levels and improved hepatic antioxidant capabilities and reversed alcohol-induced steatosis.

In addition, it is understood that excessive reactive oxygen species (ROS) can oxidate zinc-finger motifs, resulting in a loss of DNA binding.[58] The annotated GO biological process term "reactive oxygen species metabolism" was identified as a significant molecular function (Figure 2). Furthermore, up-regulation of several ROS-related genes, such as glutathione peroxidase 2 (*Gpx2*), aldehyde dehydrogenase 3b1 (*Aldh3b1*), monoamine oxidase a (*Maoa*), and NADPH quinone oxidoreductase 1 (*Nqo1*) was observed (Table 2), implying high levels of ROS may have been present. Future work must elucidate the connection between Zn depletion and altered zinc-finger activity by oxidative stress. It may be that oxidative stress from chronic alcohol feeding (and potentially from PCB126 exposure) displaces Zn bound to cysteine residues in zinc fingers to disrupt transcriptional regulation.[59]

Other metals of note, such as Mg and Co, were also significantly lower in the EtOH+PCB126 group relative to controls. Mg functions as a cofactor in a plethora of enzymes, and researchers have observed the depletion of this metal in ALD cohorts.[60]

Table 3. MetaCore generated transcription factor analysis for the EF(veh. vs. PCB126) comparison ($n = 6$ vs. 6), sorted by highest z-score.

Order	Gene name	Actual[a]	n[b]	R[c]	N[d]	Expected[e]	Ratio[f]	p-Value[g]	z-Score[h]
1	*Fbi1**	11,808	17,046	13,737	34,931	6,704	1.76	0	111.9
2	*Sox17*	9,239	17,046	10,086	34,931	4,922	1.88	0	102
3	*Cry1*	10,799	17,046	12,791	34,931	6,242	1.73	0	101.3
4	*Gata1**	10,044	17,046	11,643	34,931	5,682	1.77	0	99.05
5	*Lbp9*	11,846	17,046	14,997	34,931	7,318	1.62	0	97.91
6	*Klf4**	11,958	17,046	15,352	34,931	7,492	1.6	0	96.32
7	*Ets1*	7,494	17,046	7,727	34,931	3,771	1.99	0	96.02
8	*Klf17**	8,697	17,046	9,653	34,931	4,711	1.85	0	95.42
9	*Znf263**	7,695	17,046	8,200	34,931	4,002	1.92	0	93.28
10	*c-Myc*	15,080	17,046	22,564	34,931	1.10×10^4	1.37	0	91.08
11	*Hnf4α**	7,781	17,046	8,948	34,931	4,367	1.78	0	83.73
12	*Gata2**	7,990	17,046	9,311	34,931	4,544	1.76	0	83.43
13	*Cbfl*	6,751	17,046	7,366	34,931	3,595	1.88	0	82.82
14	*Tal1*	7,872	17,046	9,165	34,931	4,472	1.76	0	82.72
15	*Creb1*	6,876	17,046	7,625	34,931	3,721	1.85	0	81.76
16	*Runx1*	6,714	17,046	7,438	34,931	3,630	1.85	0	80.64
17	*Nanog*	8,089	17,046	9,759	34,931	4,762	1.7	0	79.36
18	*Gabpα*	5,131	17,046	5,228	34,931	2,551	2.01	0	77.41
19	*E2f1*	5,265	17,046	5,469	34,931	2,669	1.97	0	76.47
20	*Esrrα**	6,975	17,046	8,275	34,931	4,038	1.73	0	73.94

Note: Transcription factors with an asterisk (*) after the gene name signifies that they contain a zinc-finger domain.
[a]"Actual" means the number of targets in the activated dataset(s) regulated by the chosen transcription factor.
[b]n means the number of network objects in the activated dataset(s).
[c]R means the number of targets in the complete database or background list regulated by the chosen transcription factor.
[d]N means the total number of gene-based objects in the complete database or background list.
[e]Expected means the mean value for hypergeometric distribution ($n \times R/N$).
[f]Ratio means connectivity ratio (Actual/Expected).
[g]z-Score means z-score = (Actual − Expected)/sqrt(variance).
[h]p-Value means the probability to have the given value of Actual or higher (or lower for negative z-score). Note that all p-values in this list were calculated to be so low that the MetaCore algorithm reported "0."

Rodent and human Mg supplementation studies have demonstrated that Mg mitigates oxidative stress[61] and liver injury biomarkers.[62] Co is an integral part of vitamin B12 functionality and has also been observed to be lower in alcohol-associated cirrhotic patients.[63] Cu levels were also expected to be significantly lower in the EtOH+PCB126 group; however, these levels were only numerically lower and not significant (Table S1). Previous research demonstrated that dioxin exposure increases *Slc46a3* expression to sequester Cu in the lysosome, resulting in lower available Cu levels.[34] *Slc46a3* expression was significantly higher in the EF(Veh. vs. PCB126) dataset (Table 1); however, Cu abundance was only assessed in liver homogenates, and PCB126 effects were not significant. Although these findings do not prove causal association that PCB126 promoted ALD by depleting metals, lower levels of Zn, Mg, and Co are of note in the promotion of malnutrition or unavailability of metal micronutrients. ALD is associated with variable degrees of trace metal deficiencies, and we postulate that chemical exposures could account for some of the varying clinical observations.

Although this study is unique in that it is investigating interactions of EtOH feeding and pollutant exposure, we must report its limitations. Besides the model limitations stated in our characterization study, RNA-Seq and other described methods have clear pitfalls. First, total RNA was extracted by the commonly used phenol-chloroform extraction method, resulting in possible sample contamination with various salts, dNTPs, and phenol and thus inaccurate sequencing. However, we performed DNase digestion and XP bead cleaning of samples to minimize contaminates, which are explained in the "Methods" section. Furthermore, quality assessment of reads sequenced ranged from ∼6 million to 133 million, with alignment rates between 93% to 98%. Lower aligned reads (6–22 million) were most frequently found throughout EtOH-fed mice, but the lower alignment rates (93%–95%) were found among the pair-fed mice, which could introduce sample bias or undetected genes by means of inadequate rRNA depletion. In addition, our phosphoproteomics approach is limited because we explored only phosphorylated proteins and not the total proteome. Finally, we did not rigorously examine the potential role of differential AhR activation by PCB126 and EtOH in ALD. AhR is readily activated by dioxin-like species, like PCB126, shown by prototypical target gene induction, *Cyp1a1*.[64] AhR is famously involved in detoxification processes but also plays important endogenous roles that are ligand-specific.[65–69] We also observed that EtOH feeding alone was associated with significantly higher hepatic *Cyp1a1* levels (∼4-fold) in comparison with pair-fed+veh. control (Figure S4). EtOH has previously been shown *in vitro* and *in vivo* to influence AhR activities related to autophagy[70] and hepatic stellate cell activation[71] and to interact with the microbiome.[72] AhR activation by EtOH may be an indirect protective effect that stem from EtOH's ability to dysregulate metabolite ligands and induce oxidative stress responses.[73] Other studies have demonstrated that AhR activating gut-derived indole metabolites are protective for the liver in ALD in mice.[74] Although this study demonstrated that PCB126 and EtOH activated AhR, its role in ALD pathology must be further explored.

Conclusions

Although the public is becoming increasingly aware of environmental exposure threats, it is simultaneously important to acknowledge lifestyle interactions. Research centers are currently developing human exposome studies to incorporate and consider interactions between pollutant exposures and alcohol consumption. We previously demonstrated[26] that PCB126 promoted ALD pathology in this chronic-binge rodent alcohol feeding model. The present study's RNA-Seq approach demonstrated significant alteration of the transcriptome and assisted in the generation of two hypotheses. Our first hypothesis regarding altered phosphorylated tyrosine residues was rejected; however, GO molecular function processes from RNA-Seq data suggested that metal binding was decreased. This suggestion was tested by hepatic metals quantification, which revealed that critical metals Zn, Mg,

and Co were significantly lower in the EtOH+PCB126 group relative to controls. PCB126 may be additively promoting the loss of these essential metals, which are functional in nature and may be responsible for transcriptional alterations observed in our studies. Metal supplementation and zinc-finger activity studies are required to determine whether dietary supplementation of depleted trace metals attenuate liver disease in coexposed mice by restoring transcriptional capabilities.

Acknowledgments

The authors would like to acknowledge and thank the University of Louisville Sequencing Technology Center for library preparation, sequencing, and team: Elizabeth Hudson, Shirong Zheng, Justin Kos, and Easton Ford. In addition, the authors would like to acknowledge Dr. Irina Kirpich, Dr. Dennis Warner, and Dr. Josiah Hardesty for their support in the development and analysis of this study. Finally, the authors would like to acknowledge Daniel Wilkey for his contribution in phosphoproteome sample preparation and mass spectroscopy use.

This work was funded, in part, by the National Institutes of Environmental Health Sciences (R35ES028373, T32ES011564, K01ES033289, P30ES030283, P42ES023716, R01ES032189, and R21ES031510), National Institute of General Medical Sciences (P20GM103436, P20GM113226), and National Institute on Alcohol Abuse and Alcoholism (P50AA024337, R01AA028436).

References

1. Axley PD, Richardson CT, Singal AK. 2019. Epidemiology of alcohol consumption and societal burden of alcoholism and alcoholic liver disease. Clin Liver Dis 23(1):39–50, PMID: 30454831, https://doi.org/10.1016/j.cld.2018.09.011.
2. Witkiewitz K, Litten RZ, Leggio L. 2019. Advances in the science and treatment of alcohol use disorder. Sci Adv 5(9):eaax4043, PMID: 31579824, https://doi.org/10.1126/sciadv.aax4043.
3. Cholankeril G, Ahmed A. 2018. Alcoholic liver disease replaces hepatitis C virus infection as the leading indication for liver transplantation in the United States. Clin Gastroenterol Hepatol 16(8):1356–1358, PMID: 29199144, https://doi.org/10.1016/j.cgh.2017.11.045.
4. Hirode G, Saab S, Wong RJ. 2020. Trends in the burden of chronic liver disease among hospitalized US adults. JAMA Netw Open 3(4):e201997, PMID: 32239220, https://doi.org/10.1001/jamanetworkopen.2020.1997.
5. Julien J, Ayer T, Bethea ED, Tapper EB, Chhatwal J. 2020. Projected prevalence and mortality associated with alcohol-related liver disease in the USA, 2019-40: a modelling study. Lancet Public Health 5(6):e316–e323, PMID: 32504584, https://doi.org/10.1016/S2468-2667(20)30062-1.
6. Murthy P, Narasimha VL. 2021. Effects of the COVID-19 pandemic and lockdown on alcohol use disorders and complications. Curr Opin Psychiatry 34(4):376–385, PMID: 34016817, https://doi.org/10.1097/YCO.0000000000000720.
7. Killgore WDS, Cloonan SA, Taylor EC, Lucas DA, Dailey NS. 2021. Alcohol dependence during COVID-19 lockdowns. Psychiatry Res 296:113676, PMID: 33385782, https://doi.org/10.1016/j.psychres.2020.113676.
8. Crabb DW, Im GY, Szabo G, Mellinger JL, Lucey MR. 2020. Diagnosis and treatment of alcohol-associated liver diseases: 2019 practice guidance from the American Association for the Study of Liver Diseases. Hepatology 71(1):306–333, PMID: 31314133, https://doi.org/10.1002/hep.30866.
9. Hernandez-Tejero M, Clemente-Sanchez A, Bataller R. 2023. Spectrum, screening, and diagnosis of alcohol-related liver disease. J Clin Exp Hepatol 13(1):75–87, PMID: 36647416, https://doi.org/10.1016/j.jceh.2022.10.002.
10. Zhang R, Tang Z, Xu W, Ding Y, Zhang M, Guan Q, et al. 2022. Risk factors and protective factors for alcohol-related liver disease: a systematic review and meta-analysis. Alcohol Clin Exp Res 46(12):2128–2136, PMID: 36203342, https://doi.org/10.1111/acer.14951.
11. Mathurin P, Bataller R. 2015. Trends in the management and burden of alcoholic liver disease. J Hepatol 62(1 suppl):S38–S46, PMID: 25920088, https://doi.org/10.1016/j.jhep.2015.03.006.
12. Jomova K, Makova M, Alomar SY, Alwasel SH, Nepovimova E, Kuca K, et al. 2022. Essential metals in health and disease. Chem Biol Interact 367:110173, PMID: 36152810, https://doi.org/10.1016/j.cbi.2022.110173.
13. Baj J, Flieger W, Teresiński G, Buszewicz G, Sitarz R, Forma A, et al. 2020. Magnesium, calcium, potassium, sodium, phosphorus, selenium, zinc, and chromium levels in alcohol use disorder: a review. J Clin Med 9(6):1901, PMID: 32570709, https://doi.org/10.3390/jcm9061901.
14. Cave M, Falkner KC, Ray M, Joshi-Barve S, Brock G, Khan R, et al. 2010. Toxicant-associated steatohepatitis in vinyl chloride workers. Hepatology 51(2):474–481, PMID: 19902480, https://doi.org/10.1002/hep.23321.
15. Al-Eryani L, Wahlang B, Falkner KC, Guardiola JJ, Clair HB, Prough RA, et al. 2015. Identification of environmental chemicals associated with the development of toxicant-associated fatty liver disease in rodents. Toxicol Pathol 43(4):482–497, PMID: 25326588, https://doi.org/10.1177/0192623314549960.
16. Wahlang B, Beier JI, Clair HB, Bellis-Jones HJ, Falkner KC, McClain CJ, et al. 2013. Toxicant-associated steatohepatitis. Toxicol Pathol 41(2):343–360, PMID: 23262638, https://doi.org/10.1177/0192623312468517.
17. Day CP, James OF. 1998. Steatohepatitis: a tale of two "hits"? Gastroenterology 114(4):842–845, PMID: 9547102, https://doi.org/10.1016/s0016-5085(98)70599-2.
18. Lai I, Chai Y, Simmons D, Luthe G, Coleman MC, Spitz D, et al. 2010. Acute toxicity of 3,3',4,4',5-pentachlorobiphenyl (PCB 126) in male Sprague Dawley rats: effects on hepatic oxidative stress, glutathione and metals status. Environ Int 36(8):918–923, PMID: 19969354, https://doi.org/10.1016/j.envint.2009.11.002.
19. Klaren WD, Gadupudi GS, Wels B, Simmons DL, Olivier AK, Robertson LW. 2015. Progression of micronutrient alteration and hepatotoxicity following acute PCB126 exposure. Toxicology 338:1–7, PMID: 26410179, https://doi.org/10.1016/j.tox.2015.09.004.
20. Klaren WD, Flor S, Gibson-Corley KN, Ludewig G, Robertson LW. 2016. Metallothionein's role in PCB126 induced hepatotoxicity and hepatic micronutrient disruption. Toxicol Rep 3:21–28, PMID: 26770886, https://doi.org/10.1016/j.toxrep.2015.12.001.
21. Hardesty J, Day L, Warner J, Warner D, Gritsenko M, Asghar A, et al. 2022. Hepatic protein and phosphoprotein signatures of alcohol-associated cirrhosis and hepatitis. Am J Pathol 192(7):1066–1082, PMID: 35490715, https://doi.org/10.1016/j.ajpath.2022.04.004.
22. Hardesty JE, Wahlang B, Falkner KC, Shi H, Jin J, Wilkey D, et al. 2019. Hepatic signalling disruption by pollutant polychlorinated biphenyls in steatohepatitis. Cell Signal 53:132–139, PMID: 30300668, https://doi.org/10.1016/j.cellsig.2018.10.004.
23. Osna NA, Donohue TM Jr, Kharbanda KK. 2017. Alcoholic liver disease: pathogenesis and current management. Alcohol Res 38(2):147–161, PMID: 28988570.
24. Mastrangelo G, Fedeli U, Fadda E, Valentini F, Agnesi R, Magarotto G, et al. 2004. Increased risk of hepatocellular carcinoma and liver cirrhosis in vinyl chloride workers: synergistic effect of occupational exposure with alcohol intake. Environ Health Perspect 112(11):1188–1192, PMID: 15289165, https://doi.org/10.1289/ehp.6972.
25. Yan H, Tang W, Wang L, Huang S, Lin H, Gu L, et al. 2023. Ambient $PM_{2.5}$ components are associated with bone strength: evidence from a China multi-ethnic study. J Clin Endocrinol Metab 109(1):197–207, PMID: 37467163, https://doi.org/10.1210/clinem/dgad425.
26. Gripshover TC, Wahlang B, Head KZ, Young JL, Luo J, Mustafa MT, et al. 2022. The environmental pollutant, polychlorinated biphenyl 126, alters liver function in a rodent model of alcohol-associated liver disease. Alcohol Clin Exp Res (Hoboken) 47(1):60–75, https://doi.org/10.1111/acer.14976.
27. Bertola A, Mathews S, Ki SH, Wang H, Gao B. 2013. Mouse model of chronic and binge ethanol feeding (the NIAAA model). Nat Protoc 8(3):627–637, PMID: 23449255, https://doi.org/10.1038/nprot.2013.032.
28. Chomczynski P, Sacchi N. 1987. Single-step method of RNA isolation by acid guanidinium thiocyanate-phenol-chloroform extraction. Anal Biochem 162(1):156–159, https://doi.org/10.1016/0003-2697(87)90021-2.
29. Dobin A, Davis CA, Schlesinger F, Drenkow J, Zaleski C, Jha S, et al. 2013. STAR: ultrafast universal RNA-seq aligner. Bioinformatics 29(1):15–21, PMID: 23104886, https://doi.org/10.1093/bioinformatics/bts635.
30. Yu G, Wang LG, Han Y, He QY. 2012. clusterProfiler: an R package for comparing biological themes among gene clusters. Omics 16(5):284–287, PMID: 22455463, https://doi.org/10.1089/omi.2011.0118.
31. Bekker-Jensen DB, Bernhardt OM, Hogrebe A, Martinez-Val A, Verbeke L, Gandhi T, et al. 2020. Rapid and site-specific deep phosphoproteome profiling by data-independent acquisition without the need for spectral libraries. Nat Commun 11(1):787, PMID: 32034161, https://doi.org/10.1038/s41467-020-14609-1.
32. Andrews S. 2010. FastQC: a Quality Control Tool for High Throughput Sequence Data. http://www.bioinformatics.babraham.ac.uk/projects/fastqc/ [accessed 5 December 2022].
33. Trapnell C, Roberts A, Goff L, Pertea G, Kim D, Kelley DR, et al. 2012. Differential gene and transcript expression analysis of RNA-seq experiments with TopHat and Cufflinks. Nat Protoc 7(3):562–578, PMID: 22383036, https://doi.org/10.1038/nprot.2012.016.
34. Kim J-H, Matsubara T, Lee J, Fenollar-Ferrer C, Han K, Kim D, et al. 2021. Lysosomal SLC46A3 modulates hepatic cytosolic copper homeostasis. Nat Commun 12(1):290, PMID: 33436590, https://doi.org/10.1038/s41467-020-20461-0.
35. Rein-Fischboeck L, Pohl R, Haberl EM, Zimny S, Neumann M, Eisinger K, et al. 2017. Tubulin alpha 8 is expressed in hepatic stellate cells and is induced in transformed hepatocytes. Mol Cell Biochem 428(1–2):161–170, PMID: 28063004, https://doi.org/10.1007/s11010-016-2926-4.

36. Hu X, Li J, Fu M, Zhao X, Wang W. 2021. The JAK/STAT signaling pathway: from bench to clinic. Signal Transduct Target Ther 6(1):402, PMID: 34824210, https://doi.org/10.1038/s41392-021-00791-1.
37. Medici V, Halsted CH. 2013. Folate, alcohol, and liver disease. Mol Nutr Food Res 57(4):596–606, PMID: 23136133, https://doi.org/10.1002/mnfr.201200077.
38. He L, Vatsalya V, Ma X, Klinge CM, Cave MC, Feng W, et al. 2022. Metabolic analysis of nucleosides/bases in the urine and serum of patients with alcohol-associated liver disease. Metabolites 12(12):1187, PMID: 36557225, https://doi.org/10.3390/metabo12121187.
39. Nicoll R, Gerasimidis K, Forrest E. 2022. The role of micronutrients in the pathogenesis of alcohol-related liver disease. Alcohol Alcohol 57(3):275–282, PMID: 34491307, https://doi.org/10.1093/alcalc/agab060.
40. Beier JI, Arteel GE, McClain CJ. 2011. Advances in alcoholic liver disease. Curr Gastroenterol Rep 13(1):56–64, PMID: 21088999, https://doi.org/10.1007/s11894-010-0157-5.
41. Lin Y, Chen L, You X, Li Z, Li C, Chen Y. 2021. PAQR9 regulates hepatic ketogenesis and fatty acid oxidation during fasting by modulating protein stability of PPARα. Mol Metab 53:101331, PMID: 34474167, https://doi.org/10.1016/j.molmet.2021.101331.
42. Zhao Y. 2022. Association between apolipoprotein B/A1 and the risk of metabolic dysfunction associated fatty liver disease according to different lipid profiles in a Chinese population: a cross-sectional study. Clin Chim Acta 534:138–145, PMID: 35905837, https://doi.org/10.1016/j.cca.2022.07.014.
43. Pauter AM, Olsson P, Asadi A, Herslöf B, Csikasz RI, Zadravec D, et al. 2014. Elovl2 ablation demonstrates that systemic DHA is endogenously produced and is essential for lipid homeostasis in mice. J Lipid Res 55(4):718–728, PMID: 24489111, https://doi.org/10.1194/jlr.M046151.
44. Singh V, Huang E, Pathak V, Willard BB, Allende DS, Nagy LE. 2022. Phosphoproteomics identifies pathways underlying the role of receptor-interaction protein kinase 3 in alcohol-associated liver disease and uncovers apoptosis signal-regulating kinase 1 as a target. Hepatol Commun 6(8):2022–2041, PMID: 35438255, https://doi.org/10.1002/hep4.1956.
45. Zhang D, Wu S, Lan Y, Chen S, Wang Y, Sun Y, et al. 2023. Essential metal mixtures exposure and NAFLD: a cohort-based case-control study in northern Chinese male adults. Chemosphere 339:139598, PMID: 37480945, https://doi.org/10.1016/j.chemosphere.2023.139598.
46. McClain CJ, Barve SS, Barve A, Marsano L. 2011. Alcoholic liver disease and malnutrition. Alcohol Clin Exp Res 35(5):815–820, PMID: 21284673, https://doi.org/10.1111/j.1530-0277.2010.01405.x.
47. Kasim Baltaci A, Ozyurek K, Mogulkoc R, Kurtoglu E, Ozkan Y, Celik I. 2003. Effects of zinc deficiency and supplementation on the glycogen contents of liver and plasma lactate and leptin levels of rats performing acute exercise. Biol Trace Elem Res 96(1–3):227–236, PMID: 14716102, https://doi.org/10.1385/bter:96:1-3:227.
48. Barbara M, Mindikoglu AL. 2021. The role of zinc in the prevention and treatment of nonalcoholic fatty liver disease. Metabol Open 11:100105, PMID: 34337376, https://doi.org/10.1016/j.metop.2021.100105.
49. Cassandri M, Smirnov A, Novelli F, Pitolli C, Agostini M, Malewicz M, et al. 2017. Zinc-finger proteins in health and disease. Cell Death Discov 3(1):17071, PMID: 29152378, https://doi.org/10.1038/cddiscovery.2017.71.
50. McClain C, Vatsalya V, Cave M. 2017. Role of zinc in the development/progression of alcoholic liver disease. Curr Treat Options Gastroenterol 15(2):285–295, PMID: 28447197, https://doi.org/10.1007/s11938-017-0132-4.
51. Zhong W, Zhao Y, Sun X, Song Z, McClain CJ, Zhou Z. 2013. Dietary zinc deficiency exaggerates ethanol-induced liver injury in mice: involvement of intrahepatic and extrahepatic factors. PLoS One 8(10):e76522, PMID: 24155903, https://doi.org/10.1371/journal.pone.0076522.
52. Zhou Z, Wang L, Song Z, Saari JT, McClain CJ, Kang YJ. 2005. Zinc supplementation prevents alcoholic liver injury in mice through attenuation of oxidative stress. Am J Pathol 166(6):1681–1690, PMID: 15920153, https://doi.org/10.1016/S0002-9440(10)62478-9.
53. Kang YJ, Zhou Z. 2005. Zinc prevention and treatment of alcoholic liver disease. Mol Aspects Med 26(4–5):391–404, PMID: 16099027, https://doi.org/10.1016/j.mam.2005.07.002.
54. Morris DR, Levenson CW. 2013. Zinc regulation of transcriptional activity during retinoic acid-induced neuronal differentiation. J Nutr Biochem 24(11):1940–1944, PMID: 24029070, https://doi.org/10.1016/j.jnutbio.2013.06.002.
55. Lu H. 2016. Crosstalk of HNF4α with extracellular and intracellular signaling pathways in the regulation of hepatic metabolism of drugs and lipids. Acta Pharm Sin B 6(5):393–408, PMID: 27709008, https://doi.org/10.1016/j.apsb.2016.07.003.
56. Huang K-W, Reebye V, Czysz K, Ciriello S, Dorman S, Reccia I, et al. 2020. Liver activation of hepatocellular nuclear factor-4α by small activating RNA rescues dyslipidemia and improves metabolic profile. Mol Ther Nucleic Acids 19:361–370, PMID: 31877412, https://doi.org/10.1016/j.omtn.2019.10.044.
57. Kang X, Zhong W, Liu J, Song Z, McClain CJ, Kang YJ, et al. 2009. Zinc supplementation reverses alcohol-induced steatosis in mice through reactivating hepatocyte nuclear factor-4alpha and peroxisome proliferator-activated receptor-alpha. Hepatology 50(4):1241–1250, PMID: 19637192, https://doi.org/10.1002/hep.23090.
58. Webster KA, Prentice H, Bishopric NH. 2001. Oxidation of zinc finger transcription factors: physiological consequences. Antioxid Redox Signal 3(4):535–548, PMID: 11554443, https://doi.org/10.1089/15230860152542916.
59. Wilcox DE, Schenk AD, Feldman BM, Xu Y. 2001. Oxidation of zinc-binding cysteine residues in transcription factor proteins. Antioxid Redox Signal 3(4):549–564, PMID: 11554444, https://doi.org/10.1089/15230860152542925.
60. Winrich EJ, Tiwari H, Gala KS, Royer AJ, Parajuli D, Vatsalya V. 2023. Characterization of hypomagnesemia in alcoholic hepatitis patients and its association with liver injury and severity markers. J Clin Med 12(8):2968, PMID: 37109302, https://doi.org/10.3390/jcm12082968.
61. Markiewicz-Górka I, Zawadzki M, Januszewska L, Hombek-Urban K, Pawlas K. 2011. Influence of selenium and/or magnesium on alleviation alcohol induced oxidative stress in rats, normalization function of liver and changes in serum lipid parameters. Hum Exp Toxicol 30(11):1811–1827, PMID: 21474619, https://doi.org/10.1177/0960327111401049.
62. Poikolainen K, Alho H. 2008. Magnesium treatment in alcoholics: a randomized clinical trial. Subst Abuse Treat Prev Policy 3:1, PMID: 18218147, https://doi.org/10.1186/1747-597X-3-1.
63. Prystupa A, Błażewicz A, Kiciński P, Sak JJ, Niedziałek J, Załuska W. 2016. Serum concentrations of selected heavy metals in patients with alcoholic liver cirrhosis from the Lublin region in Eastern Poland. Int J Environ Res Public Health 13(6):582, PMID: 27304961, https://doi.org/10.3390/ijerph13060582.
64. Hu W, Sorrentino C, Denison MS, Kolaja K, Fielden MR. 2007. Induction of Cyp1a1 is a nonspecific biomarker of aryl hydrocarbon receptor activation: results of large scale screening of pharmaceuticals and toxicants in vivo and in vitro. Mol Pharmacol 71(6):1475–1486, PMID: 17327465, https://doi.org/10.1124/mol.106.032748.
65. Murray IA, Perdew GH. 2020. How Ah receptor ligand specificity became important in understanding its physiological function. Int J Mol Sci 21(24):9614, PMID: 33348604, https://doi.org/10.3390/ijms21249614.
66. Jin J, Wahlang B, Thapa M, Head KZ, Hardesty JE, Srivastava S, et al. 2021. Proteomics and metabolic phenotyping define principal roles for the aryl hydrocarbon receptor in mouse liver. Acta Pharm Sin B 11(12):3806–3819, PMID: 35024308, https://doi.org/10.1016/j.apsb.2021.10.014.
67. Tanos R, Murray IA, Smith PB, Patterson A, Perdew GH. 2012. Role of the Ah receptor in homeostatic control of fatty acid synthesis in the liver. Toxicol Sci 129(2):372–379, PMID: 22696238, https://doi.org/10.1093/toxsci/kfs204.
68. Nguyen NT, Hanieh H, Nakahama T, Kishimoto T. 2013. The roles of aryl hydrocarbon receptor in immune responses. Int Immunol 25(6):335–343, PMID: 23580432, https://doi.org/10.1093/intimm/dxt011.
69. Safe S, Jin UH, Park H, Chapkin RS, Jayaraman A. 2020. Aryl hydrocarbon receptor (AHR) ligands as selective AHR modulators (SAhRMs). Int J Mol Sci 21(18):6654, PMID: 32932962, https://doi.org/10.3390/ijms21186654.
70. Kim YS, Ko B, Kim DJ, Tak J, Han CY, Cho J-Y, et al. 2022. Induction of the hepatic aryl hydrocarbon receptor by alcohol dysregulates autophagy and phospholipid metabolism via PPP2R2D. Nat Commun 13(1):6080, PMID: 36241614, https://doi.org/10.1038/s41467-022-33749-0.
71. Zhang HF, Lin XH, Yang H, Zhou LC, Guo YL, Barnett JV, et al. 2012. Regulation of the activity and expression of aryl hydrocarbon receptor by ethanol in mouse hepatic stellate cells. Alcohol Clin Exp Res 36(11):1873–1881, PMID: 22486318, https://doi.org/10.1111/j.1530-0277.2012.01787.x.
72. Qian M, Liu J, Zhao D, Cai P, Pan C, Jia W, et al. 2022. Aryl hydrocarbon receptor deficiency in intestinal epithelial cells aggravates alcohol-related liver disease. Cell Mol Gastroenterol Hepatol 13(1):233–256, PMID: 34454169, https://doi.org/10.1016/j.jcmgh.2021.08.014.
73. Dong H, Hao L, Zhang W, Zhong W, Guo W, Yue R, et al. 2021. Activation of AhR-NQO1 signaling pathway protects against alcohol-induced liver injury by improving redox balance. Cell Mol Gastroenterol Hepatol 12(3):793–811, PMID: 34082111, https://doi.org/10.1016/j.jcmgh.2021.05.013.
74. Kouno T, Zeng S, Wang Y, Duan Y, Lang S, Gao B, et al. 2023. Engineered bacteria producing aryl-hydrocarbon receptor agonists protect against ethanol-induced liver disease in mice. Alcohol Clin Exp Res (Hoboken) 47(5):856–867, PMID: 36871955, https://doi.org/10.1111/acer.15048.